Electron confinement effects on Ni-based nanostructures

2003 J. Phys.: Condens. Matter 15 S2547

(http://iopscience.iop.org/0953-8984/15/34/306)

INSTITUTE OF PHYSICS PUBLISHING JOURNAL OF PHYSICS: CONDENSED MATTER

J. Phys.: Condens. Matter **15** (2003) S2547–S2574 PII: S0953-8984(03)64402-4

Electron confinement effects on Ni-based nanostructures

J-Y Veuillen[1], **P Mallet, L Magaud and S Pons**

LEPES-CNRS, BP 166, 38042 Grenoble Cedex 9, France

E-mail: veuillen@grenoble.cnrs.fr

Received 2 June 2003
Published 15 August 2003
Online at stacks.iop.org/JPhysCM/15/S2547

Abstract

Scanning tunnelling microscopy (STM) and scanning tunnelling spectroscopy (STS) are very efficient techniques for studying confinement effects on nanostructured surfaces. Noble metal (Cu, Ag, Au) and near-noble metal (Ni, Pd, Pt) (111) surfaces present a dispersive surface state (the Shockley state) that allows a direct investigation of these effects in real space. Both the energy spectrum and the spatial distribution of the wavefunctions can be investigated using spectroscopic imaging techniques. We present a very simple model for the confinement of surface states which is sufficient to perform a first-order analysis of our experimental data on two kinds of surface resonators (quantum boxes and linear resonators). We summarize the different acquisition modes in STM/STS that allow the study of the confinement effects via the mapping of the local density of states. These points are illustrated for the well-known case of the Cu(111) surface. The main difference between Ni-based nanostructures and similar objects on the clean Cu(111) surface is that d states are present in the energy range where the Shockley surface state is expected. We report a combined experimental and theoretical analysis of the dispersion of the surface state on the clean Ni(111) surface and on a mixed Ni–Cu(111) phase (β phase). In both cases the analysis of the electronic structure of the surface is possible only in situations of strong confinement. The presence of d states is found to affect the characteristics of the Shockley state, which opens interesting perspectives.

(Some figures in this article are in colour only in the electronic version)

1. Introduction

In the last few years there has been a renewed interest in the study of Shockley-like surface states on the (111) surfaces of noble metals. This is at least in part due to the possibility to probe directly in real space their electronic properties by scanning tunnelling microscopy

[1] Author to whom any correspondence should be addressed.

(STM) and scanning tunnelling spectroscopy (STS). This allows a detailed investigation of several fundamental concepts in solid state physics. Work in this field began about ten years ago with the observation of quantum mechanical interference patterns surrounding defects on the Cu(111) [1] and Au(111) [2] surfaces. Since then, confinement effects have been studied in objects of nanometric size, obtained by various techniques: adatom manipulation [3–5], thermal deposition [6, 7] and chemical modifications [8]. One-dimensional confinement between naturally occurring parallel steps on the surface has also been reported [9]. More recently, with the development of low temperature instruments, the interest has focused mostly on two other topics, namely the study of adatom–surface interactions and the detailed analysis of the lifetime of excited states. In the first category, one can mention (among others) detailed investigations of the Kondo effect at and around isolated magnetic impurities deposited at the surface of noble metals [10–13] and the observation of an interaction between adatoms mediated by the surface state [14, 15]. The lifetime of excited electrons and holes in the surface state band can be analysed by STM using various experimental procedures [4, 5, 16, 17], including the use of confinement effects.

In this paper, we shall be mainly interested in confinement effects in Ni-based nanostructures. To be specific, we present the results that we have obtained on islands of nanometric size made of pure Ni or which consist of a Ni atomic plane inserted in a subsurface position in a Cu crystal (hereafter called β islands). As in the case of noble metal surfaces, the confinement of Shockley-like states is detected by STM/STS on these objects. The characteristics of these states obtained from *ab initio* band structure calculations are used to analyse the experimental data. The motivations for studying such surface states on structures that contain Ni are related to the presence of d states in the vicinity of the Fermi level in both cases. Since the d states are found in an energy range where the surface states are expected (at variance with the case of noble metals where the d states are well below the Fermi level), one can investigate their influence on the physical properties of the Shockley states. For instance, the dispersion of these s–p surface states can be modified by coupling with the d states [18–20], or the presence of d states around the Fermi level can affect the lifetime of the excited surface electron [21]. Additionally, in the case of Ni(111), a magnetic splitting of the surface state in one minority and one majority band has been reported [22]. This offers in principle the possibility to observe quantum mechanical interferences and confinement effects associated with each spin channel separately (since they should have a different wavelength at a given energy) which could be a new way to realize spin-polarized measurements [23]. For the case of the β phase, the insertion of the Ni plane in a subsurface position in a Cu(111) crystal should modify the energy of the Cu(111) surface state to some extent (see, e.g., [24]). This will change the electronic density in the surface state band without modifying the elemental composition of the outermost atomic plane, and therefore may help to clarify the role played by the surface state in the adsorption phenomena and in the interaction between adatoms. Notice that modification of the dispersion of the Cu(111) surface state by adsorption has already been reported [25, 26], but in these works the atomic structure of the surface plane was also modified.

The outline of this paper is as follows. In section 2, the main features of the Shockley surface states will be presented. In section 3, we shall give an introduction to confinement effects using the very simple 'hard wall' model. Although it is sufficient for the purpose of this paper, we shall also discuss briefly the refinements of this model. Our techniques for creating the nano-objects are presented in section 4. The different acquisition modes used to analyse confinement effects by STM/STS on nanostructures are presented in section 5. Section 6 gives technical details on the computational procedure and on the experimental set-up. In section 7, we illustrate the points presented in sections 2–5 for the case of the Cu(111) surface, for which the characteristics of the surface state are well known and where quantum

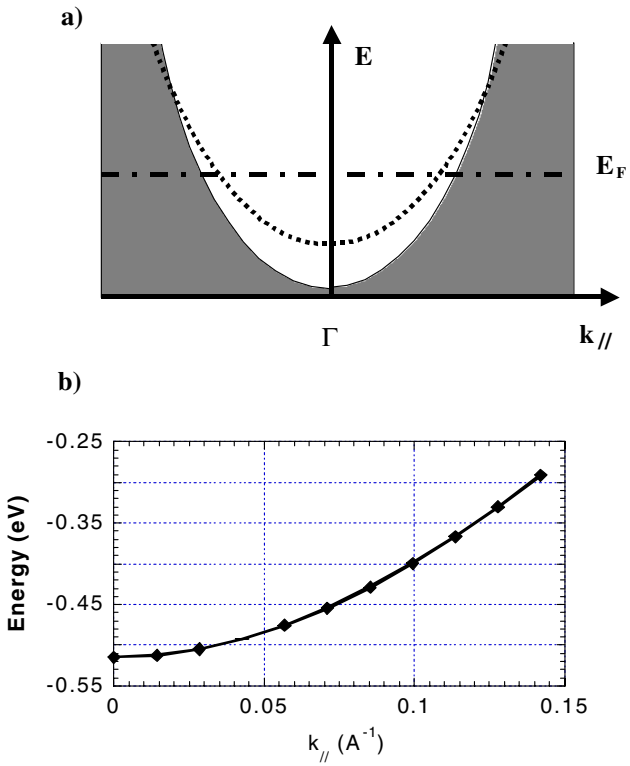

Figure 1. (a) Schematic view of the band structure of a noble metal (111) surface in the vicinity of the Fermi level E_F. The white area represents the gap of the bulk projected band structure and the dotted curve is the Shockley surface state band. E is the energy and $k_\parallel$ is the parallel wavevector in the SBZ. For Cu(111), the energy range depicted is approximately ± 1 eV and the $k_\parallel$ range is about ± 0.5 Å^{-1}. (b) Dispersion along ΓM of the Shockley state from our *ab initio* band structure calculations at the bottom of the band. We show only the average of the two split surface bands.

interferences and confinement effects have been unambiguously demonstrated. This is a very helpful introduction to sections 8 and 9, where our results on Ni-based nanostructures are presented (on Ni(111) in section 8 and on the β phase in section 9). A short conclusion is given in section 10.

2. Shockley-like surface states

The electronic states which are relevant for the confinement effects presented in this paper are the so-called 'Shockley' surface states. They form a particular class of surface states and have been extensively studied on the low index surfaces of the noble metals Cu, Ag and Au (see [27] for a review). In the next paragraph, we shall only summarize the main features of the Shockley state for the case of a noble metal (111) surface. Theoretical treatments (at various levels of complexity) that describe the physical origin of such states can be found in [27–29].

The bulk band structure of noble metals projected on the surface presents a partial energy gap near the Fermi level at the centre Γ of the surface Brillouin zone (SBZ) in the case of the (111) crystal face. For Cu(111), this 'sp' gap extends from 0.9 eV below the Fermi level to about +4.0 eV above the Fermi level at the Γ point. The lower part of this gap is schematically

depicted in figure 1, where only the energy range within 1 eV from the Fermi level is represented (this is the relevant energy range for the experiments reported here). The surface projected bulk band structure is shown in dark grey and the gap in white. Inside this gap, the Shockley surface state band is shown as a dotted curve. From photoemission data, it is located at about −450 meV below the Fermi level at the Γ point for Cu(111) and disperses upwards with increasing value of the parallel wavevector $k_{\parallel}$ [30, 31]. The dispersion of this state is isotropic and parabolic and it can be described by a bidimensional (2D) free-electron-like behaviour:

$$E = E_0 + \frac{\hbar^2 k_{\parallel}^2}{2m} \tag{1}$$

where E_0 is the bottom of the band and $m = m^* m_e$ is the effective mass of the electron in the surface state band (m_e is the free-electron mass). Experimentally, for Cu(111), $E_0 \approx -450$ meV (at low temperature) and $m^* \approx 0.4$, which leads to a Fermi wavelength of 2.9 nm. Eventually, the Shockley state disperses out of the projected bulk gap at some energy above the Fermi level and becomes a resonance [32]. The measured dispersion of the surface state can be reproduced quite accurately by first-principles electronic structure calculations (see [33]). We show in figure 1(b) the dispersion relation of the Shockley state obtained in our group from a symmetric supercell made of 15 Cu atomic layers and 6 vacuum planes. This calculation confirms that the dispersion of the state is isotropic and parabolic, with parameters $E_0 = -510$ meV and $m^* = 0.37$, in good agreement with the experimental data. Note that the size of the supercell has to be taken large enough in this slab calculation in order to avoid the coupling of the two surfaces [33], which would otherwise lead to a significant splitting δ of the surface state. (δ is 40 meV with the 15 Cu layer slab of figure 1(b), but it increases to 200 meV if only 9 Cu layers are considered. The curve of figure 1(b) is the average of the two weakly split states.)

The wavefunction associated with this Shockley state is spatially localized at the surface of the sample, inside the crystal by the bulk energy gap and outside the crystal by the vacuum barrier. For Cu(111), at the Γ point, the modulus squared of the wavefunction (i.e. the density probability) has a decay length of about 1.75 atomic layers inside the crystal [27, 34]. It has minima close to the atomic positions [27, 34]. Parallel to the surface, it behaves like a free-electron-like wave characterized by a parallel wavevector $\boldsymbol{k}_{\parallel}$ in the SBZ: $\varphi_{k_{\parallel}}\{\boldsymbol{r}\} \propto \exp(\mathrm{i}\boldsymbol{k}_{\parallel} \cdot \boldsymbol{r})$, where $\boldsymbol{r}$ is the coordinate in the surface plane.

Shockley surface states are also found on the (111) surface of near-noble transition metal surfaces Ni, Pd and Pt [27]. For the Ni(111) surface, partially occupied d states located close to the Fermi level occupy the lower part of the sp (partial) bulk bandgap at the Γ point [35]. Calculations [36, 37] and experiments [22] suggest that the Shockley state is located very close in energy from the boundary of the bulk projected bandgap (including d states) at the bottom of the band, within at least 1 eV. Note that, for symmetry reasons, the Shockley state cannot couple to bulk states at Γ, and therefore it is a true surface state at the SBZ centre even though it is degenerate in energy with the bulk d states (this is not strictly true off Γ) [22, 27]. On the experimental side, two groups have observed this dispersive Shockley state [22, 38] for Ni(111). As for Cu(111), the band shows an upwards dispersion with an essentially parabolic and isotropic dispersion, at least at the bottom of the band. However, the dispersion parameters of this state (E_0 and m^*) deduced from these electron spectroscopy experiments differ substantially. Although both groups find the bottom of the band slightly below E_F ($E_0 \approx -100$ meV [38]), the effective masses m^* reported in [22, 38] are 0.40 and 0.14, respectively. Additionally, the existence of a magnetic splitting of the surface state into a minority and a majority band (and the magnitude of this splitting) remains somewhat controversial [22, 38] in the experimental studies. Recent theoretical computations

give two spin-split surface states, with an exchange splitting that amounts to 140 meV [36] or 350 meV [37] and a band onset located just below the Fermi level for the majority component.

3. Confinement of surface states

3.1. Quantum interferences

As mentioned in the preceding section, Shockley-like surface states can be considered in a first approximation as forming a two-dimensional (2D) electron gas [39–41]. On a perfect and infinitely extended surface, the eigenstates in this model can be approximated by 2D plane waves [39–41]. However, native defects (step edges, impurities) are always present on a real surface. Alternatively, defects can be intentionally created on perfect areas of the sample. When an electron (plane) wave encounters such a defect, for instance a straight step, it will be (at least partially) coherently reflected. The reflected (scattered) wave interferes with the incident wave, giving rise to a standing electron wave ψ. $|\psi|^2$ is not uniform in space and oscillates as a function of the distance from the step. Accordingly, the LDOS at any given energy above the band onset will show periodic spatial modulations decaying away from the step edge [1, 2, 42]. Since the LDOS is a quantity to which the STM is directly sensitive (see section 5), these oscillations can be observed readily in real space [1, 2]. From the analysis of the variations of the wavelength of the spatial modulations with the bias voltage, it is possible to recover the dispersion of the surface state [1, 2, 43] (although some deviations can eventually be found, depending on the acquisition mode [44, 45]). It has also been shown [46] that the Fourier transform of low bias images gives an image of the Fermi surface in reciprocal space.

3.2. Confinement effects

In the experimental situations to be described below (Ni-based nanostructures), the Shockley-like surface states are confined into 'resonators'. This means that there are well-defined portions of the sample, delimited by step edges or by artificially fabricated atomic structures [3], from which surface state electrons are prevented from escaping, at least partially. When the characteristic length of the confining structure is of the order of the wavelength associated with the surface state electrons, the electronic structure inside the resonator is expected to be significantly different from that of the open surface (confinement effect) and the differences should show up in the STM data even at moderate energy resolution (as in the present case). To get an order of magnitude, the Fermi wavelength of surface state electrons are 2.9 and 7.85 nm for Cu(111) and Ag(111), respectively [31], which gives a characteristic length of a few nanometres for the observation of strong confinement effects. The simplest model to describe the confinement effects is the ideal confinement, or 'hard wall', model. In this case, the electrons are trapped in the resonator by infinite potential barriers (in other words, the resonator behaves as an infinite potential well). This very simple approach forms the basis for the analysis of our experimental results. We shall present the main features of the model in the next two paragraphs. More elaborate treatments of the problem will be presented at the end of the section.

3.2.1. Confinement in a box; hard wall model. Let us consider a rectangular box of length L ($\|\mathrm{O}x$) and width a ($\|\mathrm{O}y$), in which a 2D electron gas is confined by infinite potential barriers. This imposes that the amplitude of the wavefunctions must be zero on the borders of the rectangle. This boundary condition selects the energies of the eigenstates. The electron

states are labelled by two (non-zero) integer numbers n and p. The energies of the states are given by

$$E_{n,p} = E_0 + \frac{\pi^2\hbar^2}{2m}\left(\frac{n^2}{L^2} + \frac{p^2}{a^2}\right) \tag{2}$$

with the associated wavefunction $\psi_{n,p}(x, y) = u \sin(n\pi x/L) \sin(p\pi y/a)$, where $u \propto (aL)^{-1/2}$.

The electronic spectrum, integrated over the whole rectangle, consists of discrete (and infinitely sharp) levels. In practice, these levels have a finite width, as discussed in section 3.3. The LDOS at a point (x, y) inside the box consists of the same peaks centred at $E_{n,p}$ weighted by $|\psi_{n,p}(x, y)|^2$. As a consequence, the peak at energy $E_{n,p}$ should disappear from the LDOS on the nodal lines of $\psi_{n,p}(x, y)$. Conversely, the LDOS at the energy $E_{n,p}$ will show strong spatial modulations, given by $|\psi_{n,p}(x, y)|^2$. In the case of a confined 2D free-electron gas, the number of nodal lines of $\psi_{n,p}(x, y)$ increases with energy and the associated LDOS pattern becomes more complex. An experimental realization of the rectangular box that illustrates these effects is presented in [4]. All the features described for the rectangular resonator (discrete energy spectrum, spatially modulated LDOS) are common to confinement effects in boxes of various simple geometrical forms (circles [3], hexagons [6]).

3.2.2. Confinement in a linear resonator. Let us consider a strip on the surface of width $a(\|\mathrm{O}y)$, into which the surface state electrons are confined by two infinite one-dimensional potential barriers $\|\mathrm{O}x$. The electrons are free to move $\|\mathrm{O}x$, but the boundary condition (wavefunction $\equiv 0$ on the border of the strip) leads to a quantification of the wavevector k_y in the direction y (perpendicular to the strip), of the form: $k_y = n\pi/a$, where n is a positive (non-zero) integer. The electronic structure of the linear resonator therefore consists of a set of one-dimensional subbands (due to the free propagation along Ox), with onset energies E_{0n} imposed by the discrete values of k_y:

$$E_{0n} = E_0 + \frac{\pi^2\hbar^2}{2m}\left(\frac{n^2}{a^2}\right). \tag{3}$$

The wavefunctions associated with the 1D subband of index n are of the form:

$$\psi_{n,k} \propto \sin(n\pi y/a) \cdot \exp(\mathrm{i}k_x x),$$

where k_x is the component of the wavevector parallel to the strip ($\|\mathrm{O}x$). k_x can take a continuum of values since the movement along x is not constrained.

In the hard wall model, the expression of the LDOS is

$$\rho_S(E, y) \propto \sum_{i=1}^{n} \frac{1}{\sqrt{E - E_{0i}}} \sin^2\left(\frac{\mathrm{i}\pi y}{a}\right) \tag{4}$$

where n is given by $E_{0n} < E < E_{0n+1}$ (where $n + 1$ is the index of the first subband whose onset is larger than E). The LDOS is homogeneous along Ox. One recognizes the well-known $(E)^{-1/2}$ expression of the 1D DOS for a free-electron-like gas, weighted by $|\psi_{n,k}|^2$ for each subband.

Due to the $(E)^{-1/2}$ factor, the larger term in $\rho_s(E, y)$ varies in space as $\sin^2(n\pi y/a)$. The LDOS at energy E ($E_0 < E_{0n} < E < E_{0n+1}$) will therefore present n maxima along Oy (n increasing with energy). At any given point inside the resonator, the LDOS as a function of energy will show a series of very asymmetric peaks with sharp onsets at the energies E_{0n} and a slower decrease above. Due to the $\sin^2$ term in $\rho_s(E, y)$, the amplitude of the peaks are modulated along Oy. In particular, the peaks with even index n should vanish at the centre of the resonator ($y = a/2$).

3.3. Comments on the 'hard-wall' model

In the last two sections, we have presented the confinement effects in the very crude 'hard-wall' model. It turns out that this model allows a good first-order description of the experimental data. Specifically, it has been used to retrieve the dispersion relation from the evolution with energy of the standing wave pattern close to step edges [1] and to describe the spatial LDOS modulations at the Fermi level in the 'quantum corral' [3] and as a function of energy in hexagonal Ag islands [6]. Additionally, it gives a fairly good account of the positions in energy of the main peaks of the LDOS at selected points of well defined nanostructures where confinement effects are important [3, 6]. Hence, as far as we are concerned with the study of the dispersion relation of surface states, this simple model seems to be appropriate. It suffers, however, from several limitations. In particular, one obvious drawback of this model is that it gives energy spectra that consist of infinitely narrow lines in the case of the 'quantum box' (and diverging LDOS for 1D resonators), whereas high resolution experimental data show peaks with a finite energy width that is not limited by the resolution of the instruments [3, 4, 6]. This is due to the neglect of two effects that tend to restore a finite width for the discrete levels of the box.

The first phenomenon is that the confinement into real resonators is not perfect. For instance, upon reflection on the edge of the confining structure, part of the electron wave can be transmitted across the border. This decreases the amplitude of the reflected wave, and accordingly the amplitude of the spatial modulations of the interference pattern [40]. A less intuitive effect is that on the boundary of the box the surface state electrons can be scattered into bulk states [41, 47]. For the case of the scattering on a straight step edge (for instance, in a linear resonator), this is due to the fact that bulk states exist at the same energy as the surface state (see figure 1) and that the component of the wavevector perpendicular to the step is not necessarily conserved upon reflection [48] (the component of the wavevector $\parallel$ to the step is conserved). This allows a 'mixing' of surface and bulk states at the boundary of the resonator. Both effects result in a finite linewidth for the energy levels of a 'quantum box'. This can be easily demonstrated in a one-dimensional model (Fabry–Perot-like model), where electrons are confined to a segment of finite length: the infinitely sharp peaks of the ideal confinement case acquire a finite width when the modulus of the reflection coefficient for the amplitude of the wavefunction r at the ends of the segments is smaller than 1 (situation of non-ideal confinement due to any one of the two mechanisms described above)[2]. An elaborate treatment of this phenomenon, in a realistic case, has been presented in [9]. The conclusion is that the (coherent) reflection amplitude at step edges is of the order of 0.5 for steps on Ag(111) for energies in the vicinity of the Fermi level. The main effect responsible for this reduced amplitude is thought to be diffusion to bulk states, in agreement with theoretical work [41, 47].

The second phenomenon to consider when discussing the width of the peaks in the spectra is the 'intrinsic' lifetime of the electronic states, which is not specific to nanostructures. When spectroscopic experiments are performed to probe the electronic energy levels of any given system, electrons are injected (removed) into (from) excited states above (below) the Fermi level. Quite generally, these excited electronic states have a finite lifetime, which is limited by several many-body effects such as electron–phonon or electron–electron interactions [40, 49]. These effects are, of course, also present in confined electronic systems and give rise to a finite lifetime for the discrete energy levels. This finite lifetime results in a finite energy width for the probed states [50]. Very appealing experiments have been performed in the last few years to determine the lifetime of electronic surface states by STM [4, 5, 16, 17], some of them using confinement effects for this purpose [4, 5].

[2] The hard-wall model corresponds to $r = 1$.

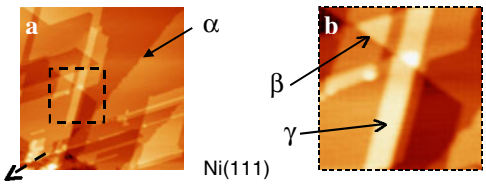

Figure 2. Topographic images of the Ni(111) surface after a nanoindentation process at sample temperature of 40 K. (a) The dotted arrow indicates the direction to the centre of the indentation (the distance to the centre is about 250 nm), while α is a step edge already existing before the indentation. Size of the image: 90×90 nm^2. (b) Zoom into the central part of (a), indicated by the broken square (size: 30×30 nm^2) which shows nanoscale islands induced by the indentation: (γ) linear island, (β) triangular island. The step edges of these nanostructures are more regular than a normal step edge α in (a).

Finally, a limited instrumental resolution also trivially leads to a finite value of the experimentally measured energy width of the electronic levels in confined geometries. For instance, in the case of the STM technique, a high temperature T for the tip leads to an instrumental resolution (full width at half-maximum (FWHM)) of about $3.5\ k_{\mathrm{B}}T$, which is of the order of 100 meV for $T = 300$ K. This is significantly larger than the linewidths measured with low temperature (high resolution) instruments operating at 4 K on nanostructures with a typical size of the order of 10 nm, which are in the range from 10 to 50 meV FWHM [3, 4, 6]. When using a 'hot' STM tip, which is actually the case in our experimental set-up, the interesting but subtle broadening mechanisms mentioned above are masked by the thermal effect. In this case, a 'hard-wall' model for the confinement, taking into account the instrumental resolution, appears to be sufficient to analyse the data. As mentioned above, this way of analysing the data has been shown previously to be efficient if one is concerned primarily with the dispersion characteristics of the surface state that gives rise to the LDOS modulations.

4. Elaboration of resonators

In order to observe the confinement effect of the Shockley surface state on (111) noble metal surfaces, nanostructures with a typical lateral size in the nanometre range have to be fabricated (see section 3). Moreover, these resonators should have a simple geometrical form to facilitate the analysis of the data. A number of strategies have been used for this purpose. Probably the most versatile one is atom manipulation [51], where adatoms are moved in the surface plane using the STM tip to delimit closed portions of the surface. 'Quantum corrals' of arbitrary shape built with various kind of adatoms can be fabricated in this way [3–5]. It requires a very low temperature instrument (typically 4 K) since otherwise surface diffusion [52] would destroy the confining structure. Another approach is to employ crystal growth techniques [52], and to select the substrate temperature and the incident atomic flux and dose to form islands with the appropriate size distribution [6]. This is basically the technique we have used to grow mixed Ni/Cu(111) 'resonators' (section 9). Finally, various kind of chemical treatments, such as bombardment with N atoms, can result in a mass production of confining structures [8].

To observe confinement effects on the clean Cu(111) and Ni(111) surfaces, we have systematized an 'indentation technique' that produces locally a large number of resonators with very well defined shapes. It consists simply in dipping the tip on the surface by performing a single inertial approach step beyond the tunnelling distance (with feedback loop disabled). The result is shown in figure 2. On the border of a strongly perturbed area, one finds a number of linear and triangular resonators, with typical lateral size in the nanometre range and one

(or more) atomic layers high (see the profile in figure 7). Specifically, β and γ in figure 2(b) denote triangular and linear resonators. The steps that define the edges of these resonators are perfectly straight, whereas native steps of the Ni(111) surface (α in figure 2(a)) have a more wavy appearance. Objects like β and γ are thus well adapted for studying confinement effects. We believe that the formation of these perfectly straight steps results from bulk atomic planes slipping one on the other in response to the stress induced by the tip during the indentation process. These structures are stable at the low temperature of the experiment (typically 40 K) either on Cu(111) or on Ni(111). The nanoindentation process often damages the apex of the tip, which can be restored by performing field emission treatment a few 100 nm's away from the analysed area.

5. Scanning tunnelling microscopy

5.1. General

The primary use of the scanning tunnelling microscope is surface imaging. This 'topographical' mode of the instrument consists generally in scanning the surface of the sample with the tip by means of piezoelectric motors. A bias V is applied between the tip and the sample, so that a current ('tunnelling current') flows between the two electrodes when they are separated by a few ångströms. The vertical position of the tip z (the tip surface distance) is adjusted for each lateral position (x, y) of the tip with respect to the sample surface using an electronic feedback mechanism in order to keep the tunnelling current constant. The 'constant current', 'topographic' or 'closed feedback loop' image of the surface is the map of $z(x, y)$. In an elementary model in which the tunnelling current depends only on the tip–sample distance (neglecting any effect of the electronic structure of the sample), a constant current image reflects faithfully the topography of the surface.

It is well known, however, that the electronic structure of the sample contributes to the STM images. This point has been established in the famous theoretical paper of Tersoff and Hamann [53]: in the limit of low bias V, at low temperature T and for an s-wave tip, the tunnelling current at a given lateral position (x, y) is directly proportional to the LDOS of the sample surface at the Fermi level, evaluated for the bare surface at the centre of curvature of the tip. Therefore, low bias constant current images reflect directly the spatial modulations of the LDOS of the sample at the Fermi energy. For 'clean' surfaces, this allows direct imaging of the Fermi surface of surface states by Fourier transform STM [46].

The theoretical description of the tunnelling current for finite biases is a complicated issue. Model calculations [54] suggest that, for a fixed tip–sample distance, the derivative of the current with respect to the bias ($\mathrm{d}I/\mathrm{d}V$, or the normalized derivative $(V/I)(\mathrm{d}I/\mathrm{d}V)$) show structures that are closely related to features of the (local) density of states of the electrodes. Under the assumption of a constant density of state for the tip (which is not always satisfied in practice), $\mathrm{d}I/\mathrm{d}V$ spectra should then reflect the LDOS of the sample surface, at least at low bias [54, 55]. This is for energies that are a small fraction of the work function of the electrodes (typically: 4 eV). A similar result has been obtained in [44], where the quantity $\mathrm{d}I/\mathrm{d}V$ was shown to approximate quite well the sample LDOS up to energies of the order of 200 meV with respect to the Fermi level. Since the energy range we shall be interested in is typically a few hundred meV above and below E_F, we can consider that in our experiments the structures in the $\mathrm{d}I/\mathrm{d}V$ signals reproduce the main features of the sample LDOS [44, 54–56], provided the density of state of the tip is sufficiently smooth. The absence of artefacts due to the tip can be verified by taking reference spectra on large and defect-free areas of the surface.

5.2. Application to nanostructures

From the discussion of section 3, it appears that the relevant quantity for analysing confinement effects in nanostructures with the STM is the LDOS of the sample, $\rho_s(E, x, y)$, where E is the energy (relative to the Fermi level of the sample) and (x, y) are the coordinates in the surface plane. The LDOS can be studied either as a function of the energy for a given location (x, y) inside the nano-object, or at a fixed energy E as a function of the position (x, y). The former case refers to local spectroscopy, the latter one to LDOS imaging. The acquisition modes used for recording the data are presented below. For the materials of interest in the present paper (Cu(111) and Ni(111)), the onset of the surface state band is located close to the Fermi level (see section 1). The typical energy range in which the LDOS has been studied therefore extends from −500 to +500 meV, which corresponds to the first quantized energy states of the system. For these energy values, the conductance signal $\mathrm{d}I/\mathrm{d}V$ should be directly related to the LDOS modulations, as discussed in the preceding paragraph.

5.2.1. Local spectroscopy. For recording local spectra, the position of the tip (x, y, z) is kept fixed, the feedback loop is deactivated and a voltage ramp is applied to the sample between two preset value V_1 and V_2. The tunnelling current is recorded during the ramp. The 'spectrum' $\mathrm{d}I/\mathrm{d}V(V)$ can be obtained either by numerical differentiation of the $I(V)$ characteristics or directly during acquisition by a lock-in technique (we use the former procedure). The tip–sample distance during the acquisition of the spectrum is chosen by stabilizing the tunnel current at a preset value for a given bias V (usually close to either V_1 or V_2) with the feedback on before the spectrum is recorded.

5.2.2. LDOS imaging. The easiest way to record a conductance image as a function of the position (x, y) at a fixed sample bias V (which corresponds approximately to an LDOS map at energy $E = eV$, where e is the electron charge, see section 5.1) is to make a constant current image of the nanostructure with the dc bias V applied on the sample, and to use a lock-in technique to acquire the $\mathrm{d}I/\mathrm{d}V$ signal simultaneously. For doing this, a small ac voltage (typical amplitude 10 meV peak to peak) at frequency f is added to the dc bias and the component of the tunnelling current modulated at the frequency f is detected by a lock-in amplifier. The output of the lock-in is recorded as a function of the tip position to construct the conductance image. Of course, the frequency f should be chosen above the cut-off frequency of the feedback loop, but below the cut-off frequency of the current amplifier.

The conductance images recorded in this way (closed feedback loop condition) are thought to represent faithfully the spatial LDOS modulations on a nano-object only if the tip–sample distance remains constant during the scan [44, 45]. In confined systems, this is approximately true only at high energy (above, say, +200 or +300 meV, depending on the system under consideration [5, 9, 42, 45]). Actually, all the states of the sample located between the Fermi level and eV will contribute to the dc tunnelling current I. The LDOS associated with the confined states in this energy range have an oscillatory behaviour, and therefore the dc tunnelling current will be sensitive to the weighted sum of these modulations. If $eV(E)$ is large, the integration is over several eigenstates with different periodicity and the weighted sum will show only weak residual oscillations. In this case, a constant dc tunnelling current corresponds to an essentially constant tip–sample distance, and the conductance image at sample bias V is essentially similar to the LDOS map at energy E [42, 45]. But if $eV(E)$ is small, only a few eigenstates of the confined system contribute to the tunnelling current and their average still presents important modulations. In this case, the tip–sample distance will vary during the scan at constant dc current. This will result in distortions between the conductance image and the

true LDOS map at energy E [45]. The closed feedback loop conductance images are therefore not directly related to the sample LDOS at low bias, and other imaging techniques have to be applied in this energy range (say, below +200 or +300 meV).

In the limit of zero bias, the Tersoff–Hamann theory states that the STM probes the LDOS of the sample at the Fermi level [53]. Therefore, topographic images taken at a few millivolts will essentially reflect $\rho_s\ (E_F, x, y)$. For larger biases (within 200–300 meV from the Fermi level), one can use a technique derived from the current imaging tunnelling spectroscopy (CITS) [57]. It consists in taking a constant current image while controlling the tip–sample distance at large positive sample bias (above, say, +200 meV), so that the tip–sample distance remains essentially constant over the whole image. At each point of the topographic image, the feedback loop is disabled and an $I(V)$ characteristic is recorded between two preset voltages V_1 and V_2 (alternatively, a $\mathrm{d}I/\mathrm{d}V$ spectrum can be recorded directly by lock-in technique). After completion of the spectrum, the feedback loop is reactivated and the tip is moved to the next topographic point. From the whole set of $I(V)$ (alternatively $\mathrm{d}I/\mathrm{d}V$) curves, conductance $\mathrm{d}I/\mathrm{d}V$ maps for energies ranging from eV_1 to eV_2 can be constructed (by a numerical derivative in our case). This technique allows LDOS mapping at low bias (a few hundred mV), and the $\mathrm{d}I/\mathrm{d}V$ images obtained in this way can be connected to closed feedback loop conductance images and to topographic images at high and very low bias, respectively. The main advantages of this CITS acquisition mode is that it provides an LDOS map at several energies at once, and that one can extract spectra at selected points inside the resonators from the set of $I(V)$ curves. Moreover, by integrating the $\mathrm{d}I/\mathrm{d}V$ spectra over the whole resonator, one can get the total DOS of the nanostructure. The main drawback of this technique is that it is quite slow, especially if one wishes to have a good spatial resolution and $I(V)$ curves with low noise.

6. Technical details

6.1. Scanning tunnelling microscopy

We use an home-made variable temperature microscope based on the inverted beetle design. In this configuration, at the lowest achievable sample temperature (around 40 K), the STM head itself remain close to room temperature (this is shown by the invariance of the scanning range of the piezoelectric tubes with sample temperature). As a consequence, the tip remains warm (at a temperature around 300 K), which limits the energy resolution of the system (this design was initially chosen to allow fast changes of the sample temperature on a large range). We use electrochemically etched W tip, treated *in situ* by ion bombardment and annealing.

The Ni(111) and Cu(111) surfaces have been prepared by the usual procedure, that consists of cycles of Ar ions bombardment and annealing. Ni was deposited from a home-made evaporator, in which a Ni rod is heated by electron bombardment. The deposition rate (typically 1 Å min^{-1}) was calibrated before deposition using a quartz microbalance.

6.2. Ab initio calculations

Calculations have been performed within the density functional theory. The code VASP [58] uses a plane wave basis and the electron ion interaction is described in the PAW approach. This limits the size of the plane wave basis. A cut-off of 450 eV was used. Integration in the Brillouin zone is done on a set of 451 irreducible k points generated from the Monckhorst–Pack scheme. We use a symmetric supercell made of 15 atomic layers and 6 vacuum planes. This rather large cell is needed to limit the surface–surface artificial interaction as mentioned before for the case of Cu(111).

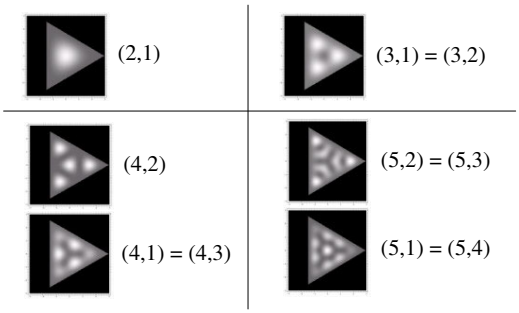

Figure 3. Density probability $|\Psi_{n,p}(x, y)|^2$ of the lowest energy eigenstates of an equilateral triangle in the hard-wall model. The shape of the triangular box appears in grey on the black background. The numbers in parentheses are the corresponding (n, p) values.

Apart from the electronic structure, the code is able to compute the relaxation of the atomic positions as well as the total energy of the supercell system. This allows the direct determination of the most stable configurations at a constant number of atoms. For instance, we obtain for the bulk copper lattice parameter $a = 3.636$ Å, in good agreement with other theoretical and experimental values.

The weight of a state is calculated from the projection of the corresponding wavefunction on spherical harmonics that are non-zero within a sphere located on the atom. Our criterion to distinguish surface states is that their weight is larger on the first two atomic layers and rapidly decreases inside the cell.

7. Confinement in Cu(111) resonators: an illustration

Before presenting results on Ni-based nanostructures, it is instructive to illustrate the preceding considerations for the case of Cu(111). The characteristics of the surface state are well known for Cu(111), and the fact that one can observe by STM quantum interferences patterns and confinement effects due to the scattering of the Shockley surface state at defects (step edges and impurities) is well established [1, 3]. We present here data for a triangular box and for a linear resonator. This will largely facilitate the discussion of the results on Ni-based nanostructures.

7.1. Triangular box

The eigenstates of a 2D electron gas confined in a equilateral triangular box have been computed analytically in [59]. They are characterized by two integer numbers n and p, with the condition $n > p \geqslant 1$. The eigenenergies are given by

$$E_{n,p} = E_0 + \frac{8\pi^2\hbar^2}{9mL^2}(n^2 + p^2 - np) \tag{5}$$

where L is the side of the triangle.

This gives a discrete energy spectrum. For the small n values that we shall consider in the following ($n < 10$), the energy of the states increases with n (whatever the value of p) and, for a given n, are the highest for $p = 1$ and $n - 1$. The associated wavefunctions have a complicated analytical form [59]. For illustration we present in figure 3 the density probability ($|\psi_{n,p}(x, y)|^2$) for the lowest energy states (n, p). The states (n, p) and $(n, n-p)$ have identical energies and density probability. One notices that some (n, p) states ((2, 1), (4, 2), (5, 1)) have a maximum at the centre whereas others ((3, 1), (4, 1), (5, 2)) have zero weight at the centre. These states will not contribute to the measured LDOS at the centre. From the

expression of $E_{n,p}$ and from figure 3, one expects to observe an increasing number of maxima and minima in the LDOS images with increasing energies. Similar probability distributions have been computed in a different context, namely for triangular structures on the InAs(111) surface [60]. Due to band bending effects, the density probability for the first eigenstates is slightly different in this latter case, but the order and the degeneracy of the levels is the same.

Our data for a triangular box formed on the Cu(111) surface (see section 4) are shown in figures 4 and 5. The side of the triangle is $L \approx 6$ nm (a topographic image is shown in figure 5(0)). Figure 4(a) displays conductance $\mathrm{d}I/\mathrm{d}V$ STM spectra extracted from a CITS image, which in a first approximation reflect the sample LDOS. On a Cu(111) spectrum taken on a terrace adjacent to the triangle (diamonds), one notices a jump in the conductance at about -450 mV, which marks the onset of the Cu(111) Shockley state at -450 meV below E_{F} [1]. Only weak structures are seen above the edge, in agreement with the expected uniform DOS of a 2D state. The spectrum integrated over the whole triangle (full line), which reflects the total DOS of the triangle, shows clear oscillations with maxima located approximately at -280, -100 and around +150/+200 mV. These maxima correspond to the energy of the first eigenmodes (2, 1), (3, 1 and 2), (4, 2) and (4, 1 and 3) that result from the confinement of the Cu(111) Shockley states into the triangle. Their respective energies computed from the above formula are -295, -100, +144 and +193 meV for $L = 6$ nm, in close agreement with the experimental values. In the spectrum taken at the centre of the triangle (dotted line), one finds again peaks at -300 and +150 mV, but the structure at -100 mV found on the integrated spectrum is essentially missing. This is due to the fact that the wavefunction associated with this state ($n = 3$) has zero weight at the centre and hence gives no contribution to the LDOS.

One remarks that the structures of the experimental spectra have a significant energy width, whereas the ideal confinement model predicts infinitely narrow width. As quoted above, this effect is essentially of instrumental origin in our case and results mainly from a hot tip. Actually, the width of the onset of the Cu(111) surface state that we measure on terraces far from defects (about 140 meV, see figure 9) is larger by $\approx$100 meV than the one reported using high resolution microscopes (about 30 meV [61]). As a consequence, the discrete peaks of the DOS can only be resolved on small triangles since $E_{n,p}$ varies as L^{-2}.

Conductance maps obtained in the CITS mode on the same triangle at selected biases are shown in figure 5. With increasing energies the number of structures in the images increases, as expected. A similar (although different in detail) effect has been reported for triangular structures on the InAs(111) surface [60]. In figure 5, the signal at the centre of the triangle is low between -150 and +10 mV, in agreement with the low intensity found in the spectrum in this energy range. The 'LDOS' images of figure 5(1), 5(2) and 5(3) look similar to the density probability of the (2, 1) and (3, 1/2) states, but the image of figure 5(4) differs from what is expected for either the (4, 1/3) or (4, 2) mode (see figure 3). This is due to the fact that the energy separation between these modes ($\approx$50 meV) is smaller than our energy resolution. Therefore, figure 5(4) is a superposition of these two modes.

We have performed a simulation of the experimental conductance spectra and images of figures 4 and 5 using a very simple model, which takes into account the finite experimental energy resolution of our STM. We consider the contribution of the 2D Shockley surface state of Cu(111) to the LDOS only (bulk states add a smooth background). The sample eigenstates are taken from the hard wall model. To reproduce the experimental resolution, we consider a tip with constant DOS and an energy distribution of the electrons in the tip given by a Fermi–Dirac type function:

$$f_{\Delta}(E) = \left(1 + \exp\left(\frac{E}{\Delta}\right)\right)^{-1} \tag{6}$$

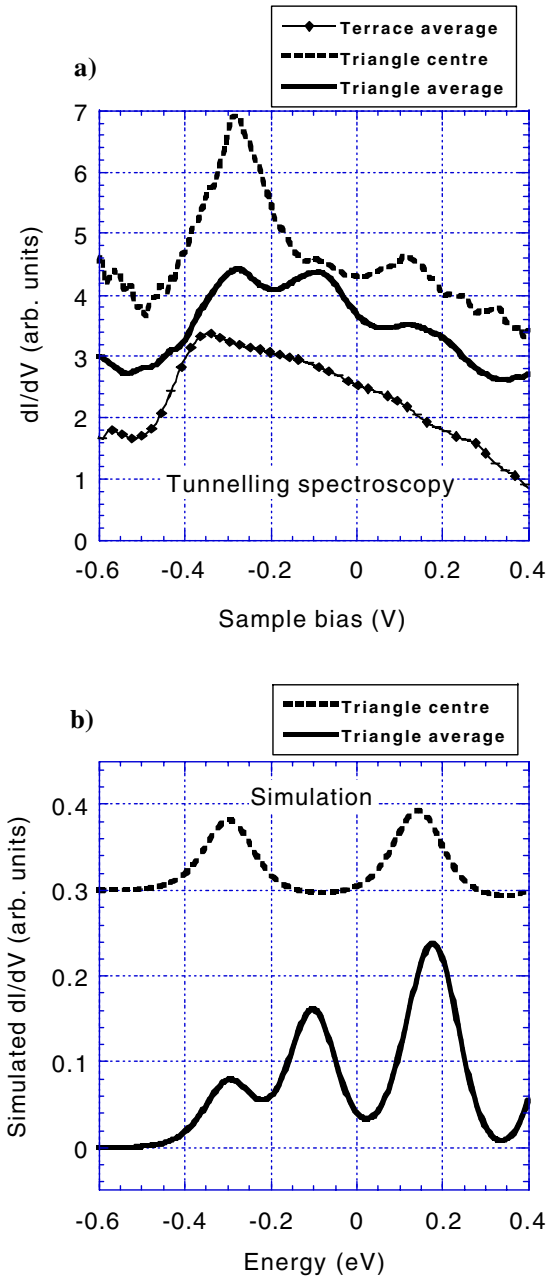

Figure 4. (a) Tunnelling conductance spectra taken on a Cu(111) terrace (diamonds) and at the centre (dotted curve) of the Cu(111) triangle shown in figure 5(0). The full curve is the spectrum integrated over the whole triangle. (All from a CITS experiment performed at a sample temperature of 40 K.) (b) Simulated integrated spectrum (full curve) and central spectrum (dotted curve) for this triangle of side $L = 6$ nm using the model described in the text. Only the surface state DOS is taken into account.

where E is the energy referenced to the Fermi level. This is equivalent to setting an effective temperature $T = \Delta / k_{\mathrm{B}}$ to the tip (the sample temperature is set to 0 K). Assuming moreover

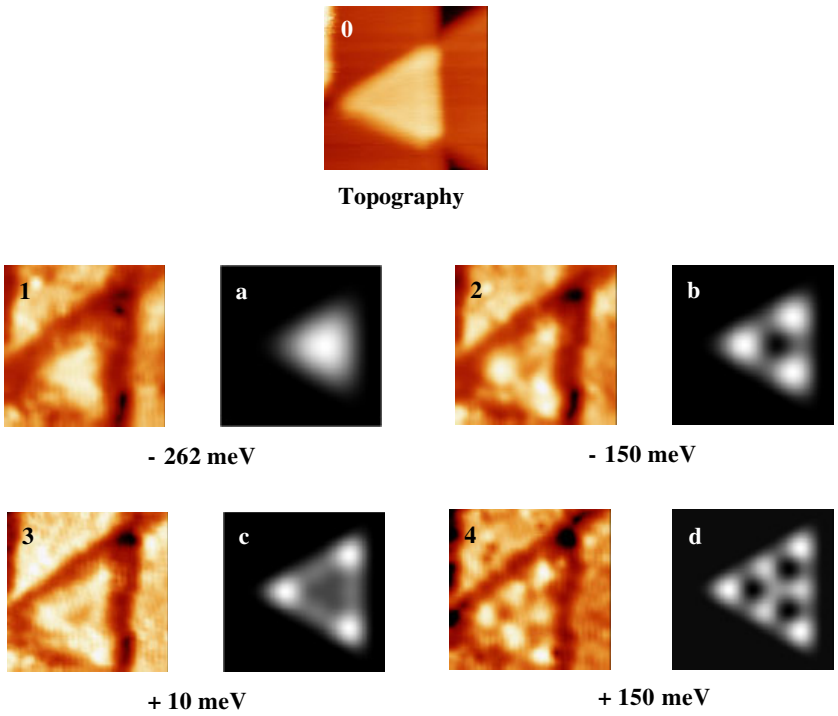

Figure 5. (0) Topographic image of an equilateral triangle of side $L = 6$ nm obtained by indentation on the Cu(111) surface (size of the image: 9×9 nm^2, bias: +1.0 V, tunnelling current: 2.0 nA). (1)–(4) Conductance ($\mathrm{d}I/\mathrm{d}V$) images of this triangle extracted from a CITS. Size of the images: 7.5×7.5 nm^2. The energies corresponding to these 'LDOS maps' are: −262 meV (1), −150 meV (2), +10 meV (3) and +150 meV (4). (a)–(d) are the simulated LDOS images (conductance maps) obtained using the model and the parameters described in the text for the same energies. The triangle appears slightly elongated in the conductance images due to a residual drift. The temperature of the sample is $T = 40$ K.

that the transmission of the tunnel barrier is approximately constant over the energy range of interest, the conductance is then given by

$$\frac{\mathrm{d}I}{\mathrm{d}V}(V, x, y) \propto -\sum_{n,p} |\psi_{n,p}(x, y)|^2 \left[\frac{\mathrm{d}f_\Delta}{\mathrm{d}E}(E_{n,p} - eV)\right]. \tag{7}$$

This is simply a weighted sum of the contributions of the different (n, p) eigenstates to the LDOS, with the weighting factor

$$-\left[\frac{\mathrm{d}f_\Delta}{\mathrm{d}E}(E_{n,p} - eV)\right]$$

which is approximately a Gaussian function centred on $E_{n,p}$ with a FWHM of 3.5Δ. The value we have chosen for Δ is 40 meV. It gives a good account for the width of the rising front of the surface state on the open terraces (at 140 meV, this is 3.5Δ) and for the width of the peaks corresponding to the discrete levels inside the triangle. This value of Δ is larger than the expected value for the thermal broadening of a tip at 300 K (25 meV) and includes other imperfections of our system, such as electronic and mechanical noise, as well as intrinsic effects (see section 3).

The result of the simulations for both LDOS imaging and local spectroscopy is shown in figures 4(b) and 5(a)–(d). The dispersion parameters of the Cu(111) Shockley state are those

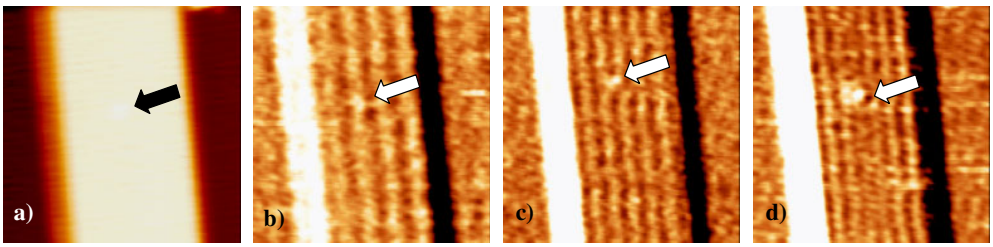

Figure 6. (a) Topographic image of a linear resonator 1 ML high formed by indentation on the Cu(111) surface at 45 K. (b)–(d) Closed loop conductance images of the same structure at biases −200 mV (b), +200 mV (c) and +400 mV (d). The arrow points to a defect on the resonator. Size of the images: 18×18 nm^2, width of the resonator: 8.7 nm.

of section 2 and we have used a slightly different form of equation that includes a transmission coefficient for the barrier. The simulated data qualitatively reproduce the experimental results. A similar level of agreement has been reached for triangles of different sizes on Cu(111) and Ag(111). This model can therefore be used with some confidence for the case of triangular islands on Ni(111).

7.2. Linear resonator

A topographic image of a linear resonator of width 8.5 nm obtained by nanoindentation is shown in figure 6(a). From the considerations of section 3 (equation (4)), we expect to find LDOS modulations perpendicular to the steps due to the scattering of the surface state electrons on the parallel edges of the resonator, with a number of minima (maxima) that increases with increasing energy above the surface band onset. This is what we observe on the closed loop conductance images of figure 6(b)–(d), where the number of bright lines across the islands changes from 4 to 6 when going from −200 to +400 mV (the very bright line on the left side is not taken into account since it includes a contribution from the step edge). We shall not perform a more detailed analysis of this data set, which is presented only to show how confinement effects show up in STM images of linear resonators. This will be helpful for the analysis of Ni/Cu nanostructures. Let us mention that the simple model described in section 7.1, which basically consists in broadening the LDOS obtained from the hard-wall model by the derivative of a Fermi–Dirac distribution reproduces fairly well the experimental data for linear resonators on Cu(111) and Ag(111) (not shown) with a similar value of Δ.

8. Nanostructures on the Ni(111) surface: confinement of the Shockley surface state

As mentioned in the introduction, the motivations for studying the surface Ni(111) are (among others): the presence of '3d' states in the energy range where the surface state exists and the possible existence of a magnetic splitting of the Shockley state. First, it is necessary to show that this surface state can be detected by STM, and to evaluate the dispersion parameters. A convenient way to do this is to analyse the variation with bias of the standing wave patterns in the vicinity of straight step edges [1]. This procedure does not work on Ni(111) due to the weakness of the signal in this case (on Cu(111) and Ag(111) we could observe clear standing wave patterns near step edges). On figure 7(a), one can see two step edges (m1 and m2) on the topographic image of a Ni(111) surface. Closed loop conductance images (this is: LDOS images, see section 5) of the same area at biases +150 and +250 mV are shown in figure 7(c) and (d). On both images, one can see a faint line parallel to each step, indicated by an arrow. The

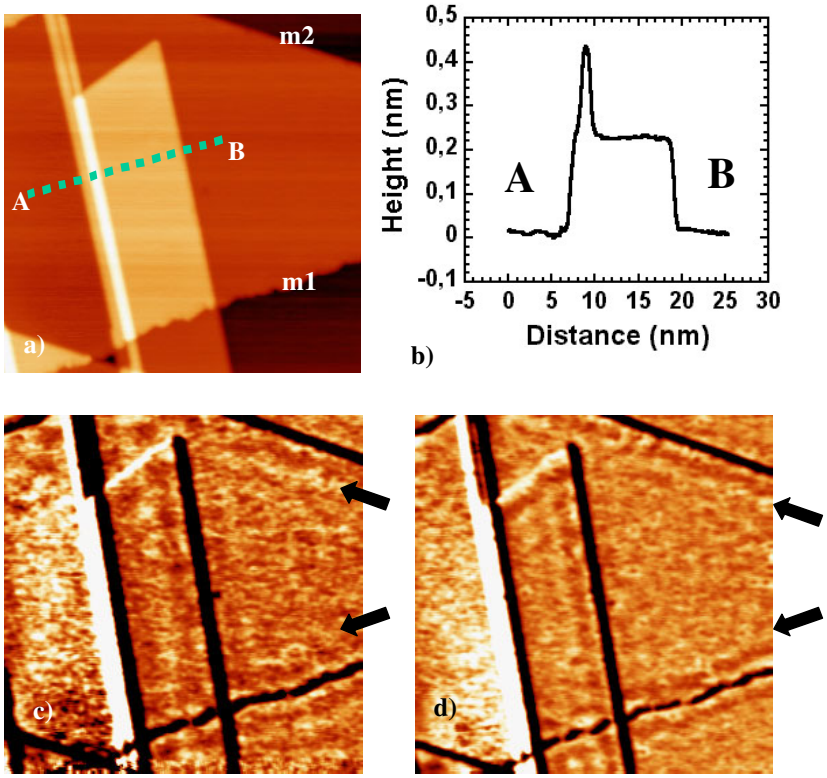

Figure 7. (a) Topographic image of the Ni(111) surface after an indentation step at 40 K. m1 and m2 denote two steps on the surface. (b) Profile along the line AB of (a), which shows that the linear resonator is 1 ML (2.1 Å) high. (c) and (d) Closed loop conductance maps of the same area as in (a) for biases +150 mV (c) and +250 mV (d). Size of the images (a)–(d): 40×40 nm^2.

position of the line relative to the step changes with increasing bias, which indicates that this maximum may well correspond to the first oscillation of a standing wave pattern resulting from the scattering of surface state electrons at the step edge. Since the distance of the maximum to the step decreases with increasing bias, the dispersion of the corresponding surface state should be positive: E increases with $k_{\|}$ as for Cu(111) [1]. The signal is weak, however, and only one maximum can be seen, which precludes the determination of the wavelength of the modulation.

On the elongated island of figure 7 (formed by the nanoindentation process, see section 4), the LDOS modulations seem to be slightly more intense than on the terraces. It is commonly observed that the LDOS modulations inside resonators are larger than on the neighbouring open surface [3, 5]. This suggests that one could increase the conductance signal by using confinement into 'quantum boxes'. We could indeed study the dispersion of the Shockley state on Ni(111) by using the triangular structures presented in section 7.1 for Cu(111).

The conductance (or LDOS) images recorded on a small triangular island of side 12.3 nm are displayed in figure 8 [62]. The topographic image is shown in figure 8(a) and the conductance images in figure 8(b)–(e). In accordance with the considerations of section 5.2, the low bias $\mathrm{d}I/\mathrm{d}V$ images have been recorded in CITS (open feedback loop) mode, whereas the high bias images have been acquired in the constant current mode (closed-feedback loop). One can clearly see modulations inside the triangle. The distance between maxima (minima)

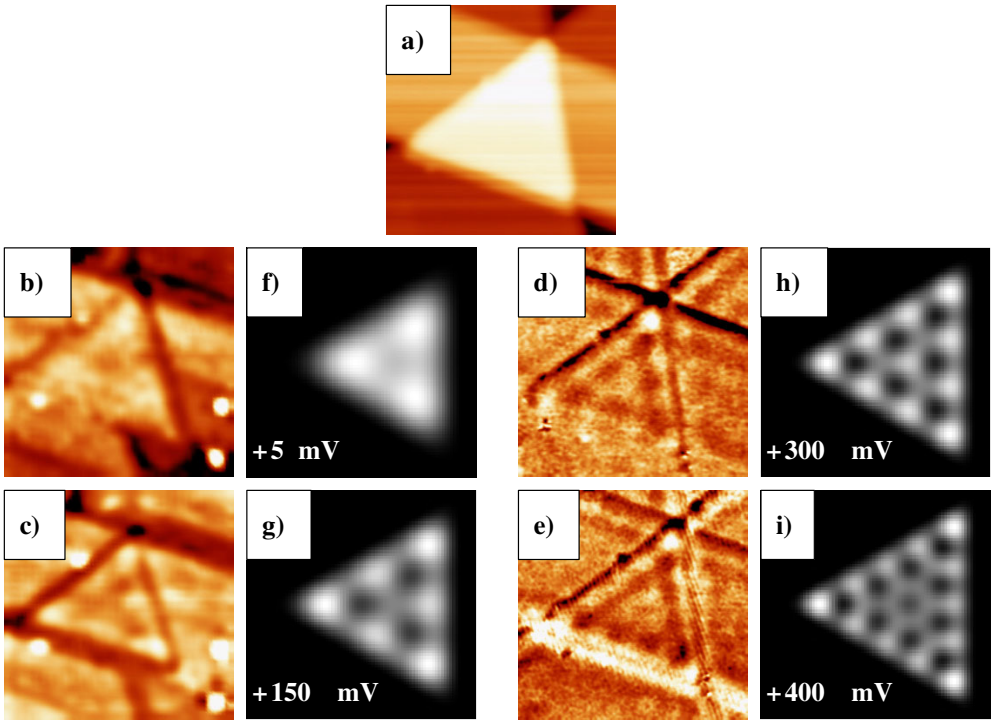

Figure 8. (a) Topographic image of a triangle created by nanoindentation on the Ni(111) surface at 45 K. (b) and (c) Open feedback loop conductance maps at +5 meV (b) and +150 meV (c) of this triangle. (d) and (e) Closed feedback loop conductance maps at +300 meV (d) and +400 meV (e). (f)–(i) Simulations of the contribution of the surface state to the conductance images inside the triangle of (a) at +5 meV (f), +150 meV (g), +300 meV (h) and +400 meV (i) using the model described in the text. From [62], © EDP Sciences 2003.

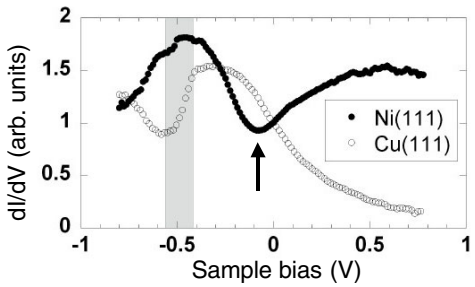

Figure 9. Differential conductance spectra acquired on large terraces (>20 nm) for Cu(111) and Ni(111) surfaces for typical sample temperatures of 45 K. The data have been normalized at $\mathrm{d}I/\mathrm{d}V = 1$ for 0 bias. The shaded box indicates the width of the rising front of the Cu(111) surface state in our experiments. The arrow points to the minimum in the Ni(111) spectrum. From [62], © EDP Sciences 2003.

decreases with increasing bias. The same behaviour was observed in conductance images of a triangle on the Cu(111) surface in section 7.1. We therefore ascribe the features in conductance maps of figure 8 to the confinement of the Shockley-like surface state of Ni(111). From the variation of the conductance pattern with bias, and in reference to figures 3 and 5, we can

immediately conclude that the dispersion of this state is actually positive (as on Cu(111)) and that the band onset is located just below E_F since what looks like the (3, 1) mode (figure 8(b)) is found at positive energy for this relatively large triangle. Since the dispersion of the surface state of Ni(111) has been reported to be isotropic and parabolic close to the Fermi level [22, 38], we can apply the model presented before for Cu(111) to extract the parameters (E_0 and m^*) of the surface state from this data set. We have done this using the same parameter Δ as for Cu(111) by varying E_0 and m^*—starting from 'reasonable' input values estimated on linear resonators—until we obtain a good agreement between the experimental images and the simulations. The result of this comparison is shown in figures 8(f)–(i) [62]. The computed images are similar to the experimental data as far as the number and position of dark/bright structures inside the triangle are concerned. The parameters of the simulation are $E_0 = -70$ meV and $m^* = 0.24$ (although these values cannot be determined with a precision better than 20 meV for E_0 and 0.04 for m^* from a visual comparison), using again $\Delta = 40$ meV. The value of E_0 is consistent with electron spectroscopy data and with theoretical computations that place the onset of the band just below the Fermi level (majority component). It is also consistent with tunnelling spectroscopy data of figure 9 where a smooth onset (indicated by an arrow) appears in this energy range. The value we find of the effective mass is intermediate between those reported in [22, 38]. Our own theoretical computations give an energy band edge $E_0 = +22$ meV and $m^* = 0.2$–0.4 for the majority component of the Shockley state close to the Γ point, in fair agreement with the present experimental data and with a previous computation [37]. We find, however, a markedly different behaviour for the minority spin electrons: the state acquires a d character and delocalizes in the bulk very fast off Γ. This is reminiscent of the predictions made in [37] for Co(0001), but not for Ni(111) where two spin-split surface states were found.

One point which deserves some comments is the weakness of the standing wave patterns observed on the Ni(111) surface compared to what is seen on Cu(111) (compare the corresponding figures 6 and 7 or 5 and 8). This behaviour may have different origins [62]:

(1) As mentioned in section 2, the Shockley state is located close to the border of the projected bulk bandgap for Ni(111). Therefore, this state will have a large attenuation length in the bulk [27] and may even be a resonance. This may reduce the weight of the Shockley state in the surface layer. One computation suggests that this state is not strongly localized in the surface plane [36].

(2) Empty d states with a high DOS exist close to the Fermi level for Ni(111). In the bulk, computations suggest that this may reduce significantly the lifetime of the excited states above the Fermi level [21]. Short lifetimes lead to a rapid attenuation of the standing wave patterns due to surface electrons away from the scattering centres [17, 40]. It is not clear, however, whether the Shockley state is sensitive to these fairly localized d states for symmetry reasons (see a comment in [32] for Pd(111)).

(3) The possible magnetic splitting of the surface state would lead to the overlap of the standing wave patterns of majority and minority states. At a given energy, theses patterns would have different periodicities (due to a different wavevector on the open surface), which would result in an overall decrease of the amplitude of the LDOS modulations. Due to the limited resolution, we are unable to decide whether one or two bands exist from our experimental data (the reported experimental splitting is smaller than the 'resolution' $3.5\Delta \approx 140$ meV). In this respect, it would be particularly interesting to confirm (or disprove) our theoretical finding of only one spin component for the Shockley state, since in that case the LDOS oscillations would be spin polarized. This is an interesting issue for spin-polarized tunnelling [23].

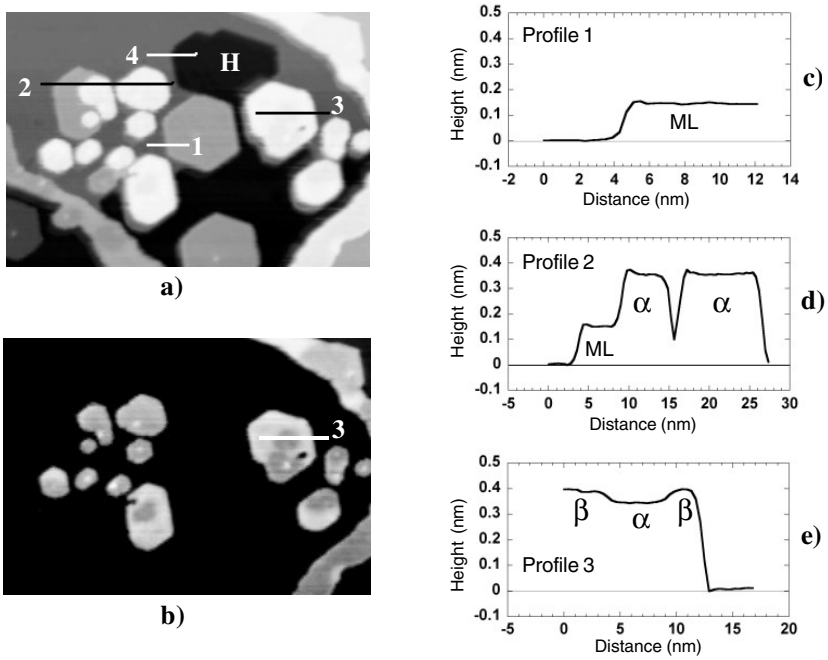

Figure 10. (From [63].) Topography of the sample surface after deposition of 0.5 ML of Ni at RT. (a) STM image, size: 73 × 51 nm^2, bias: +200 mV. The lines along which profiles 1, 2 and 3 of figures 1(c)–(e), respectively, have been taken are indicated. The profile along line 4 (not shown) indicates that structure H is located 0.2 nm below the original Cu surface. (b) Same image as (a), treated to enhance the contrast in the higher plane. (c)–(e) Profiles along lines 1, 2 and 3 of figure 1(a), respectively. The nature (ML, α, β) of the corresponding islands is indicated in the profiles. Reprinted from [63], ©2002 Elsevier Science B.V. with permission from Elsevier.

9. Hybrid Ni–Cu nanostructures: β islands

Confinement effects could be studied on another kind of Ni-based nanostrucures obtained by evaporation of Ni on a Cu(111) substrate held at 300 K. These so-called β islands consist of a Ni (or Ni-rich) atomic plane inserted in a Cu(111) crystal in a subsurface position [63]. These nano-objects grow spontaneously at room temperature after deposition of a submonolayer of Ni. Our STM study of the evolution with time of the structure of the deposit has shown that one Cu(111) plane, extracted from the surface of the free substrate, tends to cover monolayer Ni islands formed during deposition [63]. The reason for this behaviour is basically that the surface energy of Cu(111) is lower than that of Ni(111). More precisely, our first-principles calculations have shown that the energy of the configuration with a Ni plane in a subsurface position (below a Cu overlayer) is lower than the energy of the configuration where the Ni plane is laid directly above the substrate. The difference amounts to 0.215 eV/surface atom, which is close to the value computed recently by Pourovskii *et al* [64] (and from the difference between surface energies of Cu(111) and Ni(111)). A tendency towards surface segregation of Cu has actually been reported previously for Ni/Cu(111) [65].

Apart from the β islands, there exist another kind of bilayer islands, the α islands, that are made of two Ni(111) layers [63]. One also find monolayer islands (ML): this is one Ni layer on top of the Cu(111) substrate [63]. All these structures are shown in figure 10 with the corresponding profiles. One remarks that the two kinds of bilayer islands (α and β) do not have

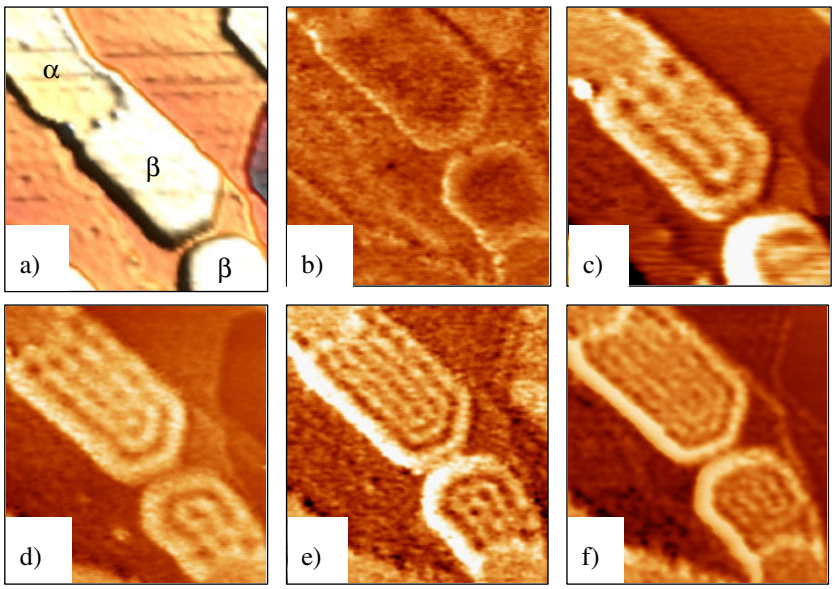

Figure 11. (From [7].) (a) Topographic image (30×30 nm^2) at 40 K of a submonolayer deposit of Ni/Cu(111). (b)–(f) Closed loop conductance images (25×25 nm^2) of the β island at the centre of (a) for increasing sample voltages: -200 mV (b), +200 mV (c), +300 mV (d), +450 mV (e) and +620 mV (f). From [7], ©2001 by the American Physical Society (with permission).

the same apparent height with STM: they differ by approximately 0.5 Å. Fully relaxed *ab initio* calculations indicate, however, that the actual (crystallographic) height of both kinds of bilayer islands should be identical within 0.05 Å. This discrepancy is ascribed to an electronic effect. The same effect is supposed to be responsible for the anomalous apparent height of the ML islands, which is about 1.5 Å or less, significantly smaller than the fully relaxed theoretical value of 2.01 Å, and also smaller than the distance between (111) atomic planes for either Ni or Cu (about 2.1 Å). A similar effect has been reported in [65]. It is noticeable that clear standing wave patterns can be observed on β islands, which have a 'normal' (i.e. close to the crystallographic value) height relative to Cu(111), whereas they are weaker (or hardly observable) on α and ML islands which have anomalous height. This supports the assumption of strong electronic effects in the topographic images.

Although standing wave patterns have been observed on both kind of bilayer islands (α and β) [7], we shall only discuss the case of β islands, for which a quantitative analysis could be performed (this is more difficult in the case of α islands due to the weaker signal and the somewhat irregular shape of the islands). Closed loop conductance images acquired at large positive sample bias are shown in figure 11. They reveal unambiguously a confinement effect on the elongated β island of figure 11(a) (width of the island $l \approx 9$ nm). This suggests that a dispersive surface state, similar in nature to the Shockley surface state of Cu(111) or Ni(111), exists on these β islands. From the evolution of the number of bright fringes across the island with increasing sample bias, we conclude that the dispersion of this state is positive, and from the absence of signal at -200 mV, one can infer that the bottom of the band is located above -200 meV. Since the LDOS modulations are essentially parallel to the long edges of the island, a first-order analysis of the data can be made using a one-dimensional model of perfect confinement (see section 3.2), at least in the central part of this structure. By simply counting the number of maxima across the island in an extended bias range (from -200 to +775 mV in

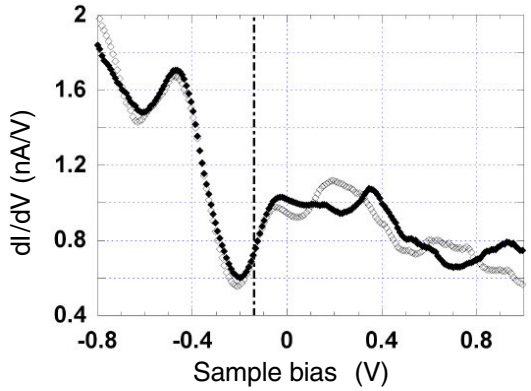

Figure 12. Tunnelling conductance spectra taken at 40 K at two different points (open and full diamonds) of the central β island of figure 11. The vertical chain line located at -140 mV indicates the middle of the rising front of the high-energy structure.

this case), we could propose the following dispersion parameters for the surface state of the β phase: $E_0 \approx -140$ meV and $m^* = 0.33 \pm 0.05$, using $a = 9$ nm (see the discussion in section 3.2) [7]. Note that we assume implicitly a free-electron-like dispersion for this surface state. We think this is justified for a first-order analysis since it is indeed the case for the pure elements Ni and Cu.

Tunnelling spectroscopy data support this value for the band edge energy E_0. Spectra taken at two neighbouring points of the β island of figure 11 are shown in figure 12. They show a peak around -450 mV and a minimum at -200 mV followed by the onset of a second structure that reaches a maximum just below the Fermi level. The middle of the rising front of this onset is located close to -140 meV (vertical chain line). The upper structure of this spectrum is thus probably due to the dispersive surface state that gives rise to the standing wave patterns of figure 11. No LDOS modulations associated with the low energy peak (at -450 mV) could be detected. The differences in the fine structure of the spectra at positive bias is probably due in part to the LDOS modulations shown in figure 11, since the two spectra have been taken at different locations inside the island.

Using the CITS technique (section 5.2), the spatial location of the spectra can be accurately determined. In figure 13(a), we show the spectrum at the centre of an elongated island of width 5 nm. The spectrum integrated on the width of this island in the central part is also displayed in this figure. Both spectra have peaks at -70 and +330 mV, due to the confinement of the surface state. A peak located around +100 mV in the integrated spectrum is absent in the central spectrum. Conductance images (not shown) indicate that these three peaks (around -70, +100 and +330 meV) correspond to the onset energies E_{0n} of the first three 1D subbands with indexes $n = 1, 2$ and 3, respectively, since 1, 2 and 3 maxima can be detected in the CITS $\mathrm{d}I/\mathrm{d}V$ maps across the islands (see section 3.2, equation (4)). The modes $n = 2$ have a minimum at the centre of the island and therefore the peak at +100 meV disappears at this place (equation (4)).

We have performed a simulation of these spectra using a model very similar to the one developed for the Ni(111) triangle. The only difference is that the LDOS of the hard-wall model (section 3.2, equation (4)) is convoluted by a Gaussian function of FWHM $= 140$ meV instead of a derivative of the Fermi function of the same FWHM. As mentioned above, both functions have very similar shape and should give essentially the same results in the simulation (we

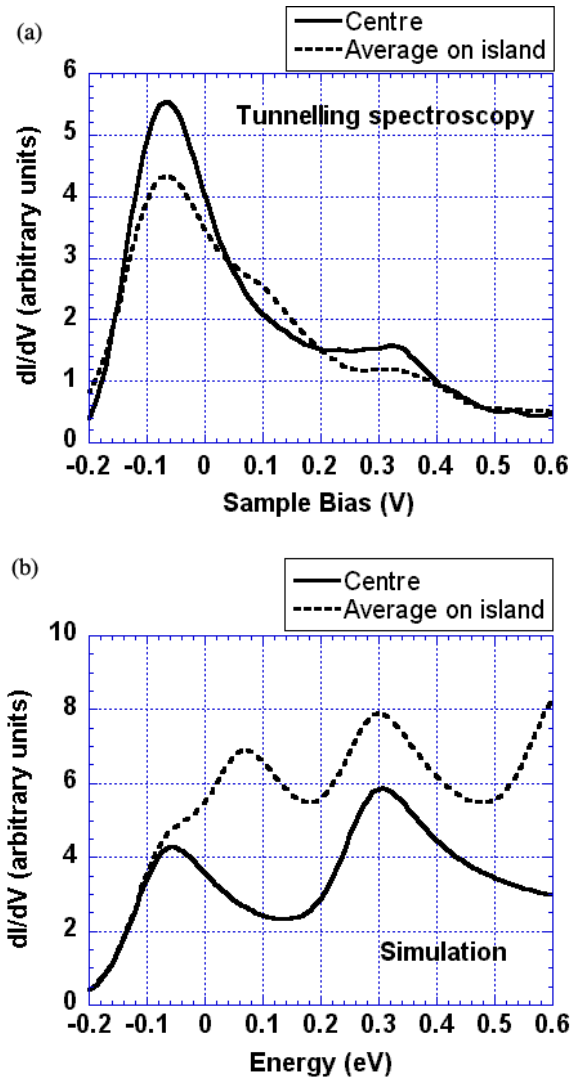

Figure 13. (a) Tunnelling conductance spectra taken at the centre of a 5 nm wide elongated β island (full curve) and integrated on the island width (broken curve). The sample temperature was 45 K. (b) Simulated spectra of the same regions given by the model described in the text.

have chosen a Gaussian for computational convenience). The result is shown in figure 13(b), using the parameters $E_0 \approx -140$ meV and $m^* = 0.33$ given above and $a = 5.0$ nm. The agreement is correct, except that the two high energy peaks appear at slightly lower energies in the simulation than in the experiment. This may be due to an overestimated value of m^*, but also to an overestimation of a (since only the product m^*a^2 appears in the expression of E_{0n}, equation (3)). Actually, reducing the width of the island to $a = 4.83$ nm (instead of $a = 5.0$ nm, as in figure 13(b)) in the simulation would give the right energy for the $n = 3$ peak. Clearly, due to the finite radius of curvature of the tip and to a possible residual drift it is experimentally difficult to discriminate between these two values from the topographic profiles. The difficulty in measuring the 'true' size of the resonators has been mentioned in [6]

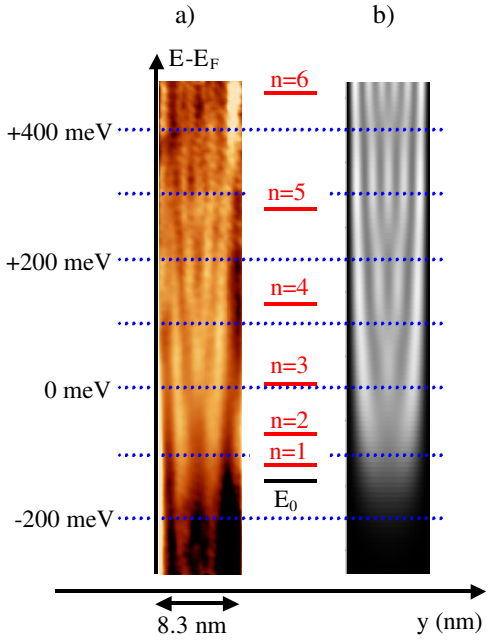

Figure 14. (a) Map of the LDOS along the width (y axis) of a linear resonator as a function of the energy referred to the Fermi level (E–E_F). The width of the resonator is $a = 8.3$ nm. The map has been reconstructed from a CITS experiment performed at 40 K. (b) Simulated LDOS map using the model and parameters given in the text. The short horizontal bars labelled 'n' indicate the position of the onsets of the one-dimensional subbands of index n in the hard-wall model with the parameters $E_0 = -140$ meV, $m^* = 0.33$ and $a = 8.3$ nm.

and it sets a limit to the accurate determination of m^* in this kind of experiment on small islands.

To decrease the relative uncertainty on a, and therefore on m^*, it is desirable to use larger resonators. However, the values of E_{0n} become more closely spaced when a increases and the corresponding peaks overlap due to the finite energy resolution. The modulations in the local spectra as a function of the bias are thus weak and it is difficult to estimate accurately the position of the maxima. It is nevertheless still possible to analyse the $\mathrm{d}I/\mathrm{d}V$ maps in this case, since spatial modulations at a given energy remain visible (which means that we analyse differences in local spectra rather than bare spectra as above). Once again, the use of the CITS mode is very helpful since it allows the acquisition of conductance images at small energy intervals on an extended energy range at once. From this set of conductance images, one can reconstruct an image of the variation of the LDOS across the linear resonator as a function of energy (the LDOS is invariant along the resonator). One such experimental image is shown in figure 14(a), taken on an island of width $a = 8.3$ nm. With increasing bias (or energy, vertical axis), one sees the appearance of successive modes with increasing n indexes, and therefore an increasing number of maxima across the island. We have simulated this map using the same model as for the spectra in figure 13, using the parameters deduced previously: $E_0 \approx -140$ meV and $m^* = 0.33$, $a = 8.3$ nm and a Gaussian broadening (FWHM = 140 meV). The result is shown in figure 14(b). Except at the very bottom of the image, the agreement between the simulated and the experimental images is very good. In particular, we can reproduce the energies at which alternately bright and dark lines appear

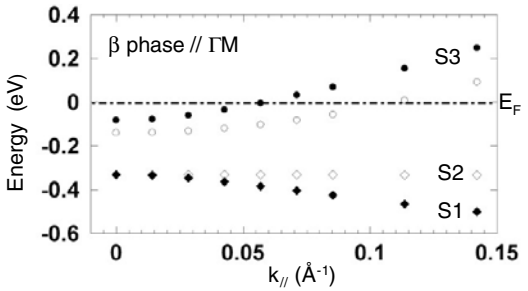

Figure 15. Computed electronic structure of the β phase along ΓM in the SBZ. Only the states in the vicinity of the Fermi level are shown. The computed bands S1, S2 and S3 are indicated by full diamonds, empty diamonds and full circles, respectively. The experimental dispersion is shown by open circles.

at the centre. The short horizontal lines labelled 'n' indicate the values of E_{0n} computed in the hard-wall model with the same parameters (equation (3)). One remarks that, due to finite energy resolution, n maxima show up in the conductance image at energies below E_{0n} (a similar effect has been reported by another group [9], but in this latter case it could be analysed in terms of imperfect confinement in the linear resonator owing to a better energy resolution).

To conclude this experimental part, we have been able to deduce the dispersion parameters of the Shockley-like surface state of hybrid Cu/Ni/Cu β islands by analysing confinement effects on nanometre scale islands. Under the assumption of a free-electron-like behaviour, the values we find are: $E_0 \approx -140$ meV and $m^* = 0.33$. The hypothesis of a parabolic dispersion seems to be approximately valid up to a few hundred millielectron volts above the band edge, since just one set of values gives a good account of the experimental data in this energy range. The effective mass m^* is comparable to the one reported for Cu(111) (about 0.4) and for Ni(111) (about 0.24, see above). The bottom of the band is shifted in energy by +300 meV as compared to the clean Cu(111) surface. As a consequence, this state is well within the bulk projected bandgap of Cu(111) and it should be strongly localized in the first surface planes. As in the case of Ni(111), the use of nanostructures is essentially an experimental trick to retrieve the electronic properties of the extended β phase here. Note, however, that, due to the peculiar formation mechanism of the β islands [63], we can only obtain small areas of this structure by room temperature deposition of Ni alone and therefore the use of nanostructures is unavoidable.

To get a better understanding of the electronic properties of the β phase, we have performed *ab initio* band structure calculations in a fully relaxed geometry. The computation has been performed in the non-magnetic case, which was found to be the most stable configuration (see also [64]). The result of the computation is displayed in figure 15, together with the free-electron-like dispersion deduced from our experiments. Only the dispersion along ΓM is shown. The behaviour along ΓK is very similar, suggesting an essentially isotropic dispersion, which was one of the assumptions we made when analysing the experimental data. Three bands S1, S2 and S3 are found close to the Fermi level. S1 disperses downwards from Γ. It has a pure Ni d character at Γ. A very small Cu p component appears with increasing values of $k_\parallel$. The state S2 is degenerate with S1 at Γ. It has a very small dispersion and a pure Ni d character in the $k_\parallel$ range considered here. S1 and S2 are located inside the gap of the projected bulk band structure of Cu(111) for the values of $k_\parallel$ shown in figure 15 [30, 31]. The S3 state is located 250 meV above S1/S2 at Γ. It disperses upwards away from Γ. It has a pure p character at Γ and it is mainly localized on the Cu surface layer with a smaller p component on the Ni

subsurface plane. Therefore this state has the characteristics of a Shockley surface state at Γ. With increasing $k_{\parallel}$, it acquires an increasing Ni d component, which becomes equal to the Cu p component for $k_{\parallel} \approx 0.15$ Å^{-1}. The bottom of the band S3 is located at −80 meV with respect to the Fermi level. Its dispersion is not actually parabolic and attempts to fit the computed results with a parabola give effective masses m^* that vary between 0.2 and 0.4, depending on the energy interval considered. From these computations, it appears that the introduction of a subsurface Ni plane in a Cu(111) crystal induces significant changes in the surface electronic structure:

(i) The Shockley state is pushed up in energy by +400 meV with respect to Cu(111). As discussed in the introduction, this effect is interesting since it modifies the electronic density in the surface state without changing the elemental composition of the surface plane. A modification of the energy of the Shockley state of Ag(111) upon insertion of an Au subsurface layer has been reported previously [24]. The effect was smaller in this latter case (≈50 meV) and interpreted as due to the perturbation induced by the difference between the Au and Ag potentials. An upwards shift of the Shockley state when a Pd monolayer is deposited (as a surface layer) on Cu(111) and Au(111) has also been observed [26].

(ii) Ni d states appear in the projected bulk bandgap of the Cu(111) face close to E_F. This is expected since the 3d band of bulk Ni is not completely filled. These states can mix with the Cu p states, as shown by the evolution of the character of the bands S1 and S3. This kind of 's–p–d' hybridization [18–20] also affects the Shockley state.

The dispersion determined experimentally using the free-electron-like model is reported in figure 15 (open circles). At first sight the agreement between experiment and theory seems rather poor, although a band with a positive (upwards) dispersion is observed in a similar energy range in both cases. The differences are not so large, however. At the Γ point, the theoretical energy of the Shockley state is only +60 meV higher in energy than the experimental one. The theoretical dispersion is steeper at the bottom of the band than the experimental one, but both curves become almost parallel at larger values of $k_{\parallel}$ (for $k_{\parallel} > 0.1$ Å^{-1}). This comes from the non-parabolic dispersion of the computed band mentioned above. Given the fact that LDA-based calculations are not expected to give exact values for the excited states and that the experimental determination of m^* is subject to some uncertainties (due, for instance, to the difficult estimation of the island width as quoted above), our opinion is that the computed band S3 actually corresponds to the dispersive state found in the experiments. If one now considers the LDOS of figure 12, the minimum found around −200 meV should reflect the gap between the S3 and S1/S2 states in the computed band structure. The S2 state, which has a pure Ni d character and that is therefore localized mostly on the subsurface Ni plane, should not contribute significantly to the LDOS measured by STM. We ascribe the low energy structure observed in the tunnelling spectra of figure 12 to the S1 state, which has a partial Cu p character of Γ. As a final remark, we notice a strong similarity between the band structure computed for the β phase (present work) and the one reported for the Ni(111) surface [37]. In both cases, one find an upwards dispersing Shockley-like state and a downwards dispersing state with a strong d character. The main differences are (i) that for the β phase both states are located well within the projected bandgap close to the centre of the SBZ and (ii) that the β phase is, in principle, non-magnetic (i.e. the bands are not spin-split).

10. Summary and conclusions

In this paper, we have presented the basic aspects of confinement effects of one specific surface state, namely the Shockley state. We have given a brief description of the spectroscopic imaging techniques of the scanning tunnelling microscope, which allow the detailed study of the confinement effects on nanostructures. We have illustrated these points in the case of triangular and linear resonators on the well known Cu(111) surface. We have observed and studied confinement effects on two different kinds of Ni-based nanostructures. They represent a peculiar case since confined geometries seem to be the only situation in which the dispersion of the surface state can be analysed. The coupling of our experimental data with *ab initio* calculations allows a better understanding of the nature of these states and opens interesting perspectives in the case of Ni(111).

Acknowledgments

This work has been partly supported by Institut de Physique de la Matière Condensée (IPMC Grenoble). We would like to thank Dr M Verdier for helpful discussions and E Dupont-Ferrier for the images of figure 6, for complementary experiments on Ag(111) and for numerical simulations.

References

[1] Crommie M F, Lutz C P and Eigler D M 1993 *Nature* **363** 524
[2] Hasegawa Y and Avouris Ph 1993 *Phys. Rev. Lett.* **71** 1071
[3] Crommie M F, Lutz C P and Eigler D M 1993 *Science* **262** 218
[4] Kliewer J and Berndt R 2001 *New J. Phys.* **3** 22.1
[5] Braun K-F and Rieder K-H 2002 *Phys. Rev. Lett.* **88** 096801
[6] Li J, Schneider W-D, Berndt R and Crampin S 1998 *Phys. Rev. Lett.* **80** 3332
Li J, Schneider W-D, Crampin S and Berndt R 1999 *Surf. Sci.* **422** 95
[7] Pons S, Mallet P and Veuillen J-Y 2001 *Phys. Rev.* B **64** 193408
[8] Leisble F M 2002 *Surf. Sci.* **514** 33
[9] Bürgi L, Jeandupeux O, Hirstein A, Brune H and Kern K 1998 *Phys. Rev. Lett.* **81** 5370
[10] Madhavan V, Chen W, Jamneala T, Crommie M F and Wingreen N S 1998 *Science* **280** 567
[11] Li J, Schneider W-D, Berndt R and Delley B 1998 *Phys. Rev. Lett.* **80** 2893
[12] Manoharan H C, Lutz C P and Eigler D M 2000 *Nature* **403** 512
[13] Knorr N, Schneider A, Diekhöner L, Wahl P and Kern K 2002 *Phys. Rev. Lett.* **88** 096804
[14] Repp J, Moresco F, Meyer G and Rieder K-H 2000 *Phys. Rev. Lett.* **85** 2981
[15] Knorr N, Brune H, Epple M, Hirstein A, Schneider M A and Kern K 2002 *Phys. Rev.* B **65** 115420
[16] Li J, Schneider W-D, Berndt R, Bryant O R and Crampin S 1998 *Phys. Rev. Lett.* **81** 4464
[17] Bürgi L, Jeandupeux O, Brune H and Kern K 1999 *Phys. Rev. Lett.* **82** 4516
[18] Harrisson W A 1979 *Solid State Theory* (New York: Dover)
[19] van Acker J F, Lindeyer E W and Fuggle J 1991 *J. Phys.: Condens. Matter* **3** 9579
[20] Song Z, Pascual J I, Conrad H, Horn K and Rust H P 2001 *Surf. Sci.* **491** 39
[21] Zhukov V P, Aryaseliawan F, Chulkov E V and Echenique P M 2002 *Phys. Rev.* B **65** 115116
[22] Donath M, Passek F and Dose V 1993 *Phys. Rev. Lett.* **70** 2802
[23] Bode M 2003 *Rep. Prog. Phys.* **66** 523–82
[24] Hsieh T C, Miller T and Chiang T-C 1985 *Phys. Rev. Lett.* **55** 2483
[25] Park J-Y, Ham D, Kahng S-J, Kuk Y, Miyake K, Hata K and Shigekawa H 2000 *Phys. Rev.* B **62** R16341
[26] Suzuki T, Hasegawa H, Li Z-Q, Ohno K, Kawazoe Y and Sakurai T 2001 *Phys. Rev.* B **64** 081403
[27] Memmel N 1998 *Surf. Sci. Rep.* **32** 91–163
[28] Smith N V 1985 *Phys. Rev.* B **32** 3549
[29] Zangwill A 1988 *Physics at Surfaces* (Cambridge: Cambridge University Press)
[30] Kevan S D 1983 *Phys. Rev. Lett.* **50** 526
[31] Reinert F, Nicolay G, Schmidt S, Ehm D and Hüfner S 2001 *Phys. Rev.* B **63** 115415

[32] Chulkov E V, Silkin V M and Machado M 2001 *Surf. Sci.* **482–485** 693
[33] Barral M A and Llois A M 2000 *Phys. Rev.* B **62** 12668
[34] Osma J, Sarria I J, Chulkov E V, Pitarke J M and Echenique P M 1999 *Phys. Rev.* B **59** 10591
[35] Himpsel F J, Ortega J E, Mankey G J and Willis R F 1998 *Adv. Phys.* **47** 511–97
[36] Mittendorfer F, Eichler A and Hafner J 1999 *Surf. Sci.* **423** 1
[37] Braun J and Donath M 2002 *Europhys. Lett.* **59** 592
[38] Kutzner J, Paucksch R, Jabs C, Zacharias H and Braun J 1997 *Phys. Rev.* B **56** 16003
[39] Crommie M F 2000 *J. Electron Spectrosc. Relat. Phenom.* **109** 1
[40] Bürgi L, Brune H, Jeandupeux O and Kern K 2000 *J. Electron Spectrosc. Relat. Phenom.* **109** 33
[41] Crampin S 2000 *J. Electron Spectrosc. Relat. Phenom.* **109** 51
[42] Jeandupeux O, Bürgi L, Hirstein A, Brune H and Kern K 1999 *Phys. Rev.* B **59** 15926
[43] Bürgi L, Petersen L, Brune H and Kern K 2000 *Surf. Sci.* **447** L157
[44] Hörmandinger G 1994 *Phys. Rev.* B **49** 13897
[45] Li J, Schneider W-D and Berndt R 1997 *Phys. Rev.* B **56** 7656
[46] Petersen L, Sprunger P T, Hofmann Ph, Laegsgaard E, Briner B G, Doering M, Rust H P, Bradshaw A M, Besenbacher F and Plummer E W 1998 *Phys. Rev.* B **57** R6858
[47] Crampin S, Boon M H and Inglesfield J E 1994 *Phys. Rev. Lett.* **73** 1015
[48] Hörmandinger G and Pendry J B 1994 *Phys. Rev.* B **50** 18607
[49] Aschcroft N W and Mermin N D 1976 *Solid State Physics* (New York: HRW International Editions)
[50] Crampin S and Bryant O R 1996 *Phys. Rev.* B **54** R17367
[51] Eigler D M and Schweizer E K 1990 *Nature* **344** 524
[52] Brune H 1998 *Surf. Sci. Rep.* **31** 121–229
[53] Tersoff J and Hamann D R 1983 *Phys. Rev. Lett.* **50** 1998
[54] Lang N D 1986 *Phys. Rev.* B **34** 5947
[55] Tersoff J and Lang N D 1993 *Scanning Tunneling Microscopy* ed J A Stroscio and W J Kaiser (San Diego, CA: Academic) pp 1–29
[56] Wiesendanger R 1994 *Scanning Probe Microscopy and Spectroscopy* (Cambridge: Cambridge University Press)
[57] Hamers R J, Tromp R M and Demuth J E 1986 *Phys. Rev. Lett.* **56** 1972
[58] Kresse G and Hafner J 1993 *Phys. Rev.* B **47** 558
[59] Krishnamurthy H R, Mani H S and Verma H C 1982 *J. Phys. A: Math. Gen.* **15** 2131
[60] Kanisawa K, Butcher M J, Tokura Y, Yamagushi H and Hiramaya Y 2001 *Phys. Rev. Lett.* **87** 196804
[61] Kliewer J, Berndt R, Chulkov E V, Silkin V M, Echenique P M and Crampin S 2000 *Science* **288** 1399
[62] Pons S, Mallet P, Magaud L and Veuillen J-Y 2003 *Europhys. Lett.* **61** 375
[63] Pons S, Mallet P, Magaud L and Veuillen J-Y 2002 *Surf. Sci.* **511** 449
[64] Pourovskii L V, Skorodumova N V, Velikov Y K, Johansson B and Abrikosov I A 1999 *Surf. Sci.* **439** 111
[65] Boeglin C, Stanescu S, Cherifi S, Deville J P, Ohresser P, Barbier A and Brookes N B 2002 *Surf. Sci.* **507–510** 522